Arctic Intense Summer Storms and Their Impacts on Sea Ice—A Regional Climate Modeling Study

Alexander Semenov [1], Xiangdong Zhang [1,*], Annette Rinke [2], Wolfgang Dorn [2] and Klaus Dethloff [2]

1   International Arctic Research Center and Department of Atmospheric Sciences, University of Alaska Fairbanks, Fairbanks, AK 99775, USA; asemenov@alaska.edu

2   Alfred Wegener Institute, Helmholtz Centre for Polar and Marine Research, 14401 Potsdam, Germany; Annette.Rinke@awi.de (A.R.); Wolfgang.Dorn@awi.de (W.D.); Klaus.Dethloff@awi.de (K.D.)

*   Correspondence: xzhang9@alaska.edu

Abstract: Various temporal and spatial changes have manifested in Arctic storm activities, including the occurrence of the anomalously intense storms in the summers of 2012 and 2016, along with the amplified warming and rapidly decreased sea ice. To detect the variability of and changes in storm activity and understand its role in sea ice changes, we examined summer storm count and intensity year-by-year from ensemble hindcast simulations with an Arctic regional coupled climate model for the period of 1948–2008. The results indicated that the model realistically simulated the climatological spatial structure of the storm activity, characterized by the storm count and intensity. The simulated storm count captures the variability derived from the National Centers for Environmental Prediction-National Center for Atmospheric Research (NCEP–NCAR) reanalysis, though the simulated one is higher than that in the reanalysis. This could be attributed to the higher resolution of the model that may better represent smaller and shallower cyclones. The composite analysis shows that intense storms tend to form a low-pressure pattern with centers over the Kara Sea and Chukchi Sea, respectively, generating cyclonic circulation over the North Atlantic and North Pacific Arctic Ocean. The former drives intensification of the transpolar drift and Fram Strait sea ice export, and the latter suppresses thick ice transport from the Canada Basin to the Beaufort–Chukchi Seas, in spite of an increase in sea ice transport to the East Siberian Sea. Associated with these changes in sea ice transport, sea ice concentration and thickness show large decreases in the Barents–Kara Seas and the Chukchi–East-Siberian Seas, respectively. Energy budgets analysis suggests that more numerous intense storms substantially decrease the downward net sea ice heat fluxes, including net radiative fluxes, turbulent fluxes, and oceanic heat fluxes, compared with that when a lower number of intense storms occur. The decrease in the heat fluxes could be attributable to an increased cloudiness and the resultant reduction of downward shortwave radiation, as well as a destabilized boundary layer induced increase in upward turbulent fluxes.

Keywords: Arctic storm/cyclone; sea ice; air–ice–sea interaction; regional modeling

1. Introduction

In conjunction with the amplified surface air temperature increase and accelerated sea ice decreases in the Arctic [1–6], the Northern Hemisphere atmospheric circulation has exhibited various pronounced changes. The most prominent manifestations include a decade-long positive trend of the Arctic/North Atlantic oscillation (AO/NAO) from the mid-1980s to the mid-1990s, followed by a spatially transformed Arctic rapid change pattern (ARP; characterized by a dipolar structure of sea level pressures with one center of action over the Eurasian high latitude and the other over the North Pacific) and a generally

poleward shift of storm tracks and intensification of Arctic storm activities [1,7–13]. Impacts of variability of and changes in the large-scale AO/NAO and ARP on surface temperatures and underlying sea ice and ocean have been extensively investigated. The results have shown that positively polarized AO/NAO has contributed to Arctic warming and sea ice reduction, and negative polarity of ARP has played a decisive role in driving the recently observed amplification of Arctic warming and acceleration in sea ice loss since the mid-1990s through various thermodynamic and dynamic processes [1,4,6,14,15].

In addition to the impacts of the large-scale atmospheric circulation forcing, synoptic scale Arctic storm activities have also demonstrated substantial influences on various aspects of Arctic sea ice properties and surface climate [8,16–18]. In particular, intense and long-lasting storms have more frequently occurred over the Arctic Ocean during recent decades [19–23]. They have obviously caused or contributed to the observed extreme events, such as the record minima of summer sea ice extent in 2012 and 2016 and the record maxima of winter surface air temperature in 2015/2016 and 2017/2018 [24–28].

Storms, serving as the fundamental weather systems on a daily basis, can impact sea ice and ocean in various complex thermodynamic and dynamic ways. It is a primary driver for transient heat and moisture transport [29,30], which may alter Arctic energy budgets. It modulates momentum and heat fluxes between the atmosphere and sea ice/ocean and, in turn, governs sea ice growth/melt, motion, and deformation. A few existing studies have examined dynamic effects of storm, showing that occurrence or passage of storms can increase sea ice velocity, generate ocean waves, and modulate sea ice export out of the Arctic Ocean. These storm-induced changes can influence sea ice distribution and mass balance [25,31–33].

Although a few studies have been conducted on aspects of storm impacts on sea ice in particular for specific cases, it is still unclear how regionally integrated storm activities have impacted sea ice changes during the past decades and what physical processes are underlying these impacts. To address this problem, we analyzed the variability of and changes in regional storm activities and associated sea ice and surface energy budgets in ensemble hindcast simulations by a fully coupled Arctic regional climate model. Considering that the number of Arctic storms climatologically reaches its maximum during summer [8,34], and the largest variability and decrease, as well as minimum value, of sea ice extent occur in summer, our analysis focused on the period from 1 July to 15 September of each year during the model simulation 61-year time period 1948–2008.

2. Model Simulation Data and Analysis Methods

2.1. Model Simulation Data

The data used for this study are from the ensemble hindcast simulations with the fully coupled Arctic regional climate model HIRHAM–NAOSIM (the High Resolution Limited Area Model (HIRLAM) dynamics with the physical parameterizations from the Max Planck Institute for Meteorology version of ECMWF global numerical weather prediction model for the atmospheric component model HIRHAM, and coupled with the North Atlantic/Arctic Ocean-Sea Ice Model NAOSIM); details about this model can be found in [35].

The model was configured to cover the entire Arctic region north of ca. 60°N at a horizontal resolution of 0.5° (~50 km) for the atmosphere and 0.25° (~25 km) for the ocean and sea ice. The model simulations cover a time period from 1 January 1948 to 31 December 2008 with 6 ensemble members. Each ensemble member was initialized using the identical atmospheric state, but perturbed ocean and sea ice conditions that were taken from different years of the preceding coupled spin-up simulation. The atmosphere lateral boundary conditions were defined by the National Centers for Environmental Prediction-National Center for Atmospheric Research (NCEP–NCAR) reanalysis dataset [36]. Details about the setup of the ensemble simulations can be found in [37].

The model simulation results were employed in a number of prior studies [37,38]. Evaluations against observations indicate that the model generally reproduces the observed summer sea-ice

variability over the past six decades, though the simulated sea-ice decline rate is relatively small compared to the observed trend during the last decade. The weaker declining trend could be attributed to the higher sea-ice volume at the beginning of the melting period in spring in the model than that in the observations [37]. The model simulations also capture feedback processes between summer sea ice and autumn atmosphere circulation with changed surface heat fluxes and boundary layer properties [38]. The results showed that negative Arctic sea-ice anomalies are associated with increased heat and moisture fluxes, decreased static stability, and modified synoptic activity and atmospheric large-scale circulation, as discussed in [39] based on observations/reanalysis (Hadley Centre Sea Ice and Sea Surface Temperature data set version 1 (HadISST1) sea-ice concentration, atmospheric variables such as sea level pressure from ERA-Interim).

2.2. Storm Identification and Composite Analysis

An improved storm identification and tracking algorithm [8] was adapted for its application to the daily sea level pressure (SLP) output of the model ensemble simulations from 1948–2008. The basic principle of this algorithm is to identify a low SLP center, which has a minimum SLP gradient of at least 0.15 hPa per 100 km with surrounding grid points. More details about this algorithm and its application on analyzing the Northern hemisphere and Arctic storm track variability and changes can be found in [8] as well as in other follow-up studies [12,33,40]. Considering the distinct geographical features and greater storm activities near the ice-free North Atlantic and North Pacific Arctic oceans during summer in climatology [8,34], we divided the Arctic Ocean into eight subregions including the Barents–Norwegian Seas, Greenland Sea, Kara Sea, Laptev Sea, East Siberian Sea, Chukchi Sea, Beaufort Sea, and Central Arctic (Figure 1).

We focused on analyzing the following two parameters to characterize the storm activity: Storm count and storm intensity. The storm count is defined as the number of storm centers in each subregion at daily time steps of the model output during the study time period. In this study, we also specifically counted intense storms, which were selected when the storm central SLP is less than 990 hPa, which is a threshold of about the 15th percentile of central SLP of all storms over the Arctic. The storm intensity, based on the method described in [8], is quantified by the reversed difference between the central SLP of the identified storm and the climatological monthly mean SLP at corresponding grid points. Therefore, positive values of storm intensity denote the negative departure of the central SLP of a storm from climatological mean SLP at this grid point.

To reveal responses of near-surface atmospheric circulation, sea ice, and surface energy budgets associated with storm activities, we conducted composite analysis of SLP, sea ice concentration, thickness, and velocity, and a net sea-ice surface energy budget based on the count of intense storms for each subregion using a criterion of ±1.5 standard deviation (σ). The positive and negative values exceeding ±1.5σ represent extreme cases with a higher and lower number of the intense storms occurring in each summer season. It is a common approach to use a certain value of σ, such as ±1.0σ, as a criterion in the composite analysis [38]. The choosing of ±1.5σ presents better composite results, assuring both the sample size large enough and reducing noises from other weather systems when the count of intense storms is relatively lower. Because the highest count of the intense storms mainly occurs over the North Atlantic Arctic Ocean (the Norwegian, Greenland, Barents, and Kara seas) and the North Pacific Arctic Ocean (the Beaufort, Chukchi, and East Siberian Seas), our composite analysis was concentrated on these two integrated subregions. We first conducted the composite analysis for each ensemble member of the model simulations and then made ensemble mean across the six ensemble members to enhance robustness of the analysis results. The Student's t-test was applied to assess the statistical significance of the difference between the composite analysis results.
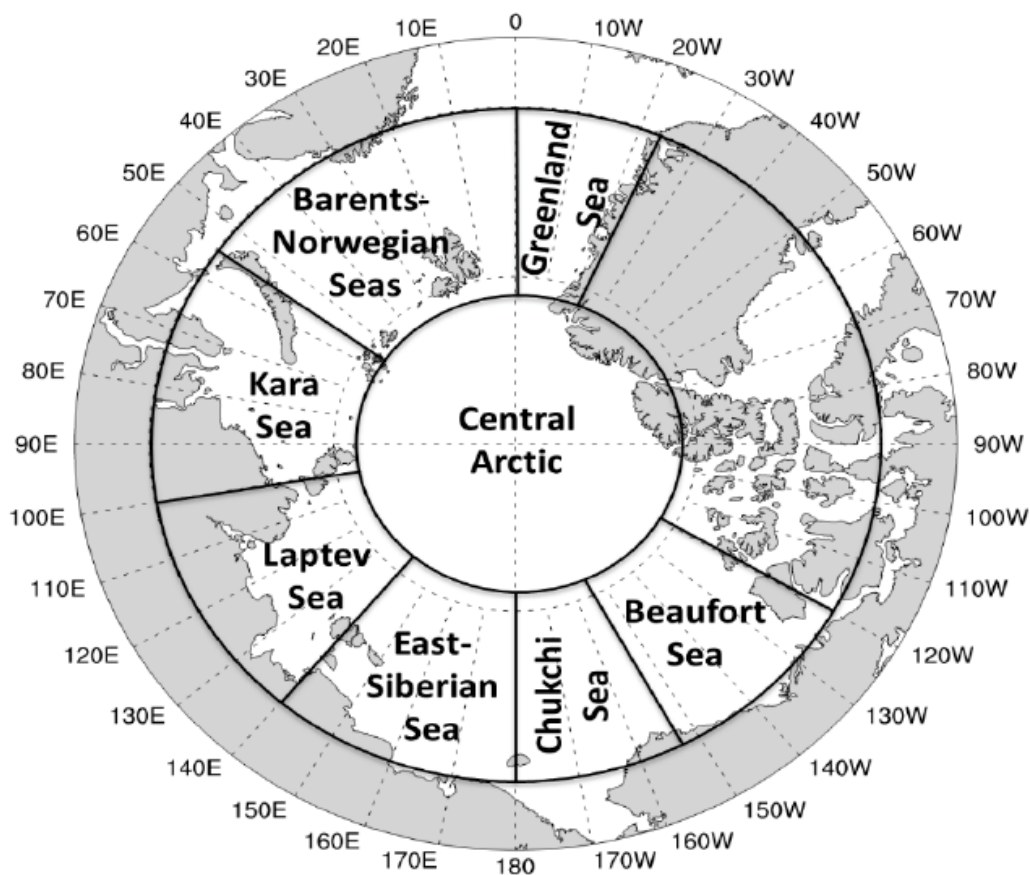
Figure 1. Division of the Arctic subregions the storm activity analysis in this study, including the Barents–Norwegian Seas (BN), Greenland Sea (GS), Kara Sea (KS), Laptev Sea (LS), East Siberian Sea (ESS), Chukchi Sea (CS), Beaufort Sea (BS), and Central Arctic (CA).

3. Results

3.1. Climatology and Variability of Summer Storm Activity

The model ensemble simulations principally capture the spatial structures of storm count derived from their forcing dataset, the NCEP–NCAR reanalysis [8,34], including the across-subregion variation (Figure 2). As was previously found [41], the total number of storms in HIRHAM–NAOSIM is higher than that in the NCEP–NCAR reanalysis. The higher storm count in the regional model could be attributed to its higher spatial resolution. Examination of impacts of model resolution on storm count and comparison of other reanalysis products with the regional model simulations has been conducted in other previous studies [42,43].

Detailed statistical analysis of the storm climatology is summarized in Table 1, including the maximum and minimum summer storm counts and the climatological mean of the summer storm count throughout the 61 years in both HIRHAM–NAOSIM simulations and the NCEP–NCAR reanalysis. The highest values of the maximum and the climatological mean storm counts occur over the Central Arctic. The maximum storm counts are comparable between the model and the reanalysis data set. However, the minimum storm counts over all subregions during the 61 years period are higher in the model than those in the reanalysis data set, which leads to the higher climatological mean storm count in the model as shown in Table 1. The higher minimum storm counts may suggest that the high resolution in HIRHAM–NAOSIM may allow better representation of smaller and shallower low-pressure systems when storm activity is weaker. The same feature was found when analyzing Arctic storms using the Arctic system reanalysis (ASR) at relatively high resolutions of 30 km or 15 km, compared to that with ERA-Interim dataset [42–45].

Table 1. The maximum, minimum, and climatological mean counts of summer (1 July–15 September) storms during 1948–2008 in HIRHAM–NAOSIM (the High Resolution Limited Area Model (HIRLAM) dynamics with the physical parameterizations from the Max Planck Institute for Meteorology version of ECMWF global numerical weather prediction model for the atmospheric component model HIRHAM, and coupled with the North Atlantic/Arctic Ocean-Sea Ice Model NAOSIM) simulations and National Centers for Environmental Prediction-National Center for Atmospheric Research (NCEP–NCAR) reanalysis.

Data Source		Central Arctic	Beaufort Sea	Chukchi Sea	East Siberian Sea	Laptev Sea	Kara Sea	Greenland Sea	Norwegian Sea	Entire Arctic
HIRHAM–NAOSIM	Max	77	19	16	26	26	26	16	36	191
	Min	33	1	2	4	3	8	2	9	95
	Ave	55	9	8	11	16	17	8	24	148
NCEP–NCAR	Max	70	21	19	21	19	28	16	35	186
	Min	2	0	0	0	0	0	0	0	10
	Ave	28	6	5	8	7	9	3	11	79
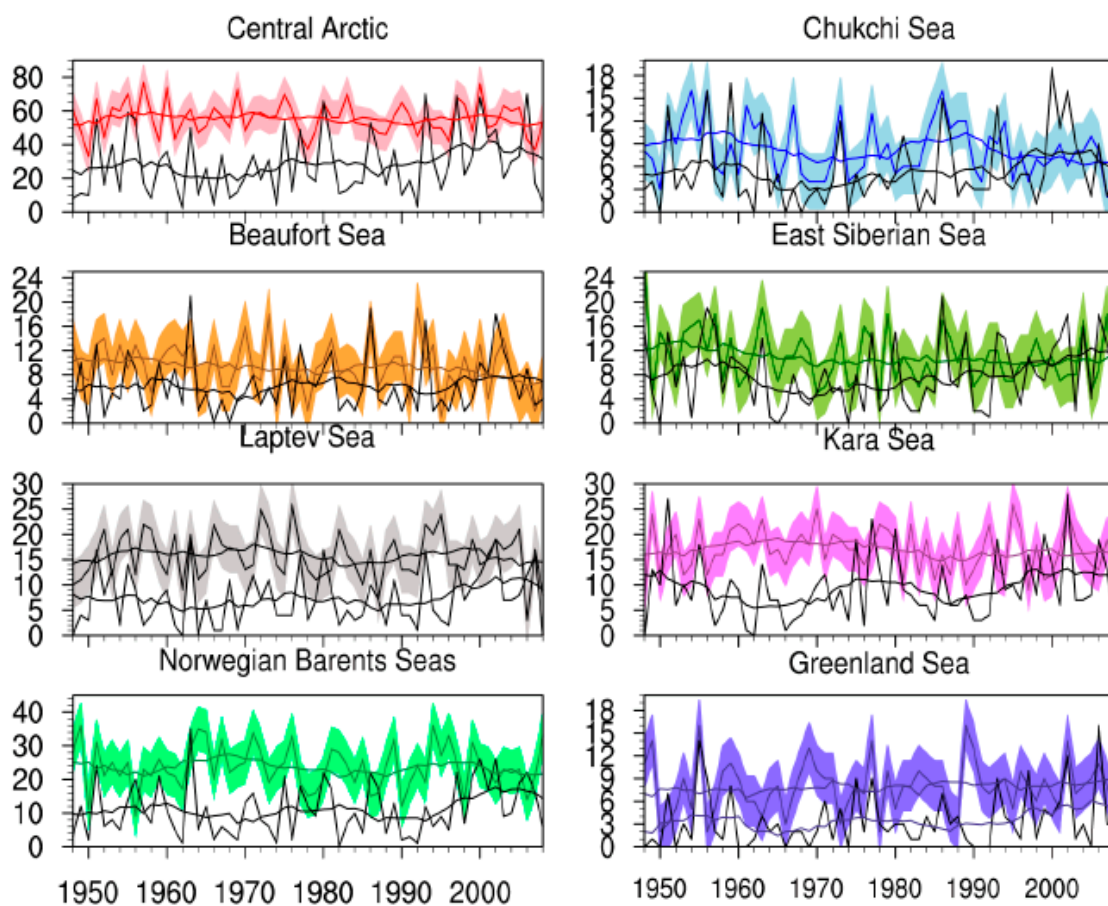
Figure 2. The storm counts derived from the HIRHAM–NAOSIM simulations and the NCEP–NCAR reanalysis dataset for each subregion for summer season (1 July–15 September) during the period of 1948–2008. The solid lines showing high-frequency variability in different colors represent the model ensemble member mean; and the shading in the color corresponding to the solid lines indicates the across-ensemble-member standard deviation. The solid black lines showing high-frequency variability demonstrate the storm counts from the NCEP–NCAR reanalysis dataset. The solid lines in color and black with low-frequency variability represent 11-year running means. Unit: Count per subregion.

Both summer storm count and intensity demonstrate obvious interannual variability throughout the study period in each of the Arctic subregions in both model simulations and the NCEP–NCAR reanalysis data (Figures 2 and 3). As expected from the climatological analysis above, the storm count is higher in the model than in the reanalysis data over the study period for all subregions. However,

the storm intensities can be close to each other for some subregions, such as the Central Arctic, Beaufort Sea, and East Siberian Sea, between the model and reanalysis. Although there are differences in the magnitude, the variability of the simulated ensemble mean of the storm counts and intensities are well consistent with that derived from the reanalysis.
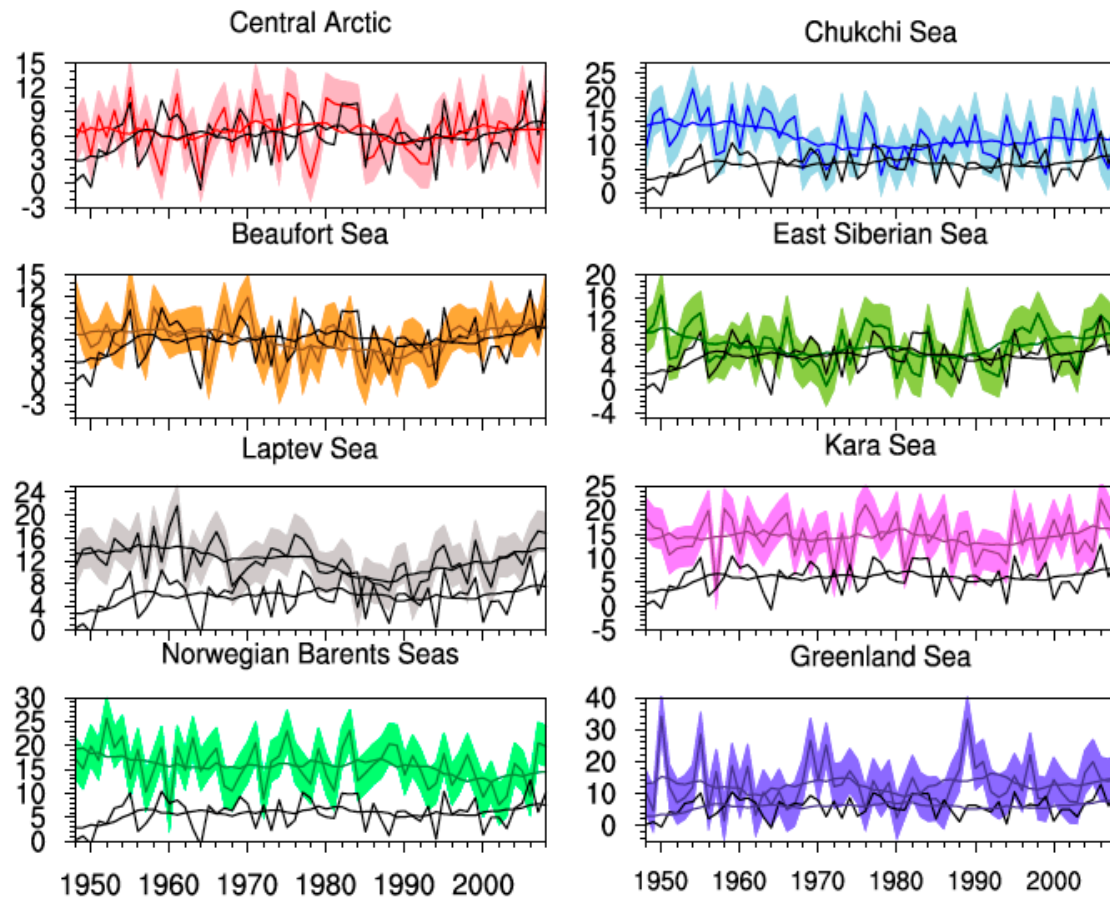
Figure 3. The same as Figure 2, but for storm intensities. Unit: hPa.

The simulated year-by-year variability of the storm count is dependent on the region, with the largest variability ranging from 33 to 77 over the Central Arctic and the smallest variability from 2 to 16 over the Chukchi Sea and the Greenland Sea (Figure 2 and Table 1). The model simulated storm intensities show relatively similar temporal variations to those in the NCEP–NCAR reanalysis. The comparison of storm intensities over the different subregions suggests that larger interannual variability occurs in the areas adjacent to open water or seasonally ice-free seas, such as the Greenland Sea and the Barents–Norwegian Sea, with the intensity ranging from 1 hPa to 40 hPa and 5 hPa to 30 hPa, respectively (Figure 3). By contrast, the Central Arctic, where almost all sea-ice cover remains during summer, exhibits the smallest magnitude and interannual variability of the storm intensity. In addition, the time series of the storm count and intensity here do not show an identifiable long-term trend. This is different from the annual mean values revealed by previous studies [8,9], which could be attributed to seasonality of the long-term changes in storm activity. Regional compensating effects may also mask the overall long-term tends over the entire Arctic as described in [46].

When comparing the regional features of the storm count and intensity discussed above, we can also readily find that the Central Arctic generally has a higher storm count but weaker storm intensity, while over the surrounding shelf seas, there are lower numbers of storms but with stronger intensity. This would be due to larger baroclinicity in the shelf seas (e.g., the Norwegian, Barents, Kara, Laptev, and Chukchi seas), resulting from the thermal contrast between open water and sea ice or between the partially sea-ice covered seas and adjacent landmass. A high resolution modeling

study on a long-lasting summer storm found that the surface and low troposphere baroclinic instability over the shelf seas is the primary mechanism triggering storm genesis and intensification, though downward intrusion of a synoptic stratospheric polar vortex or dynamically stratospheric potential vorticity anomaly plays a predominantly driving role in storm's persistence over the sea-ice covered central Arctic Ocean [22].

3.2. Intense Storms and Associated Near-Surface Atmospheric Circulation

In addition to the general information about storm activities over the Arctic, intense storms are especially interesting to examine because of their high impacts on other climate and environment components, including dramatic sea-ice changes. We therefore conducted a composite analysis of near-surface atmospheric circulation as represented by SLP and 10 m wind fields, as described in Section 2.2. Over the North Atlantic Arctic Ocean, when a higher count of the extremely intense storms occurs, the minimum mean low-pressure center appears over the Kara Sea (Figure 4a). The low pressure extends from the Kara Sea coast area to the Barents Sea, Fram Strait, and the Icelandic Sea. At the same time, a weaker Beaufort high shifts southward to the Alaska coast. This SLP allocation forms a cyclonic circulation over the Atlantic Arctic and, accordingly, favors an intensification of the transpolar drift and Fram Strait export of sea ice [4,15,47].
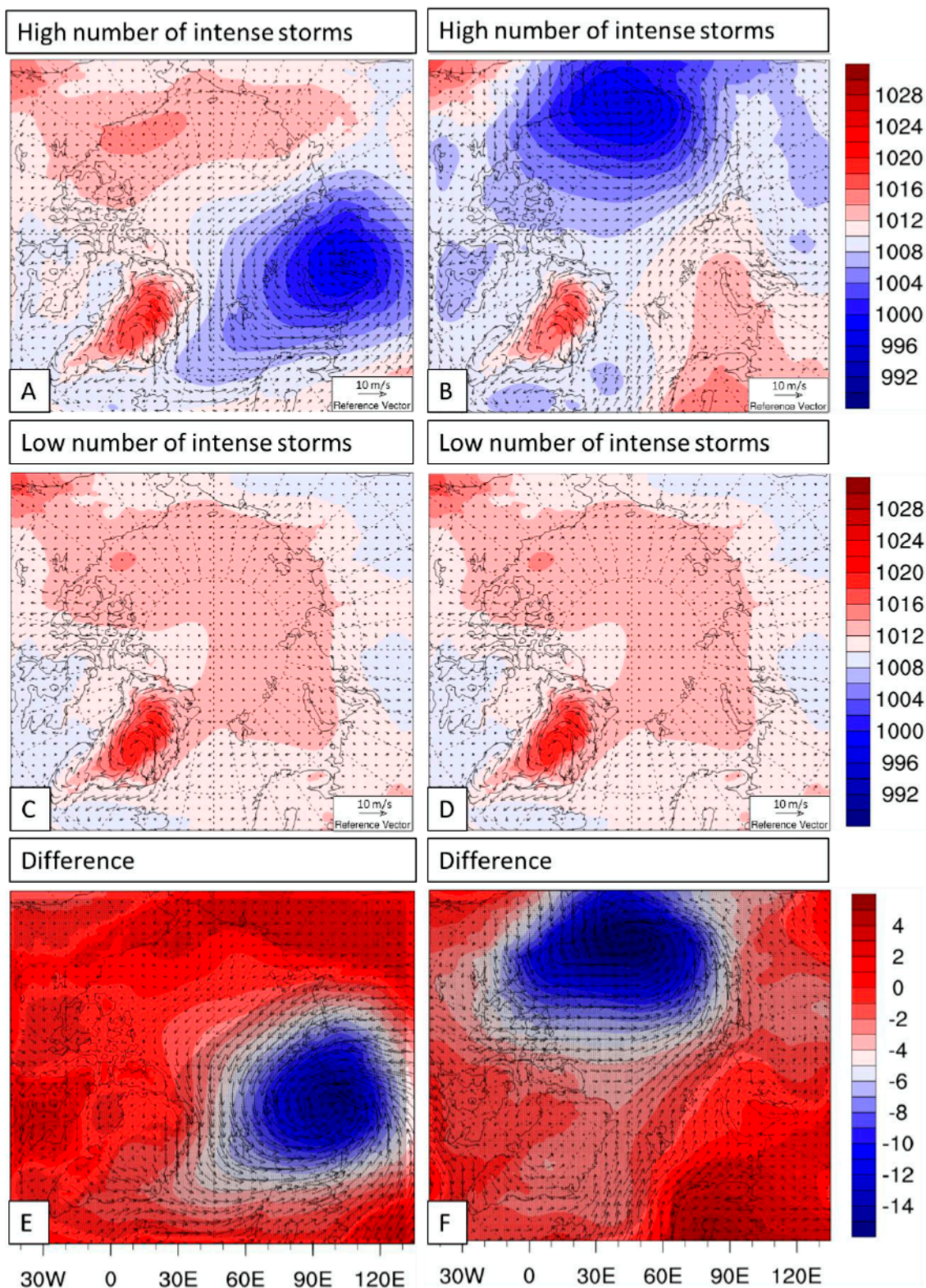
Over the North Pacific Arctic Ocean, the composite analysis results show a low-pressure center over the Chukchi Sea in the case of extremely high intense storm count. The low-pressure extends eastward to the Beaufort Sea and the Western Canadian Archipelago, and westward to the East Siberian Sea (Figure 4b). This SLP pattern alters the climatological wind field steered by the Beaufort high with wind blow from the Beaufort Sea to the Chukchi Sea [48–50]. Meanwhile, a high-pressure ridge appears from Scandinavia to the Barents Sea. As a consequence, a well-organized cyclonic circulation occurs over the North Pacific Arctic and wind blows from the Nordic Sea toward the East Siberian coast, against the transpolar drift.

To assure the impacts of the intense storms on the near-surface atmospheric circulation revealed above, we also did the same composite analysis for the days when storms occur, but the intense storm count is less than -1.5σ over the Atlantic and Pacific Arctic Ocean, respectively. The results indicate that there is no obviously identifiable SLP or circulation system over the Arctic Ocean (Figure 4c,d). Differences of composite results between the higher and lower intense storm counts reinforce the results shown in Figure 4e,f.

3.3. Changes in Sea Ice in Association with Intense Storm Activity

In correspondence to the near-surface atmospheric circulation as an integrative consequence of the intense storm activity (Figure 4), we examined the associated changes in the sea ice and ocean fields to understand possible impacts of intense storms. In this analysis, we employed the same composite analysis approach.

In the Atlantic Arctic Ocean, the difference of the composite sea-ice concentration (SIC) between the extremely high and low intense storm count shows negative values over the broad area from the Barents and Kara seas to the Greenland Sea, except for a few small spots on the downstream side of Svalbard and Novaja Zemlja (Figure 5a; see also wind pattern in Figure 4a). The largest and statistically significant SIC decrease occurs in the Northwestern Barents Sea, Southeastern Kara Sea, and Northern Greenland Sea. Sea-ice thickness (SIT) demonstrates the same decreasing pattern, but the largest decrease appears in the Northern Greenland Sea (Figure 5c). Corresponding to the decrease area of SIC and SIT, sea surface temperature (SST) exhibits an increase when more numerous intense storms occur (Figure 5e). Similarly, in the Pacific Arctic, SIC and SIT decrease in the East Siberian Sea, Chukchi Sea, and the Beaufort Sea, associated with more numerous intense storms, but increase in the Canada Basin and the Canadian Archipelago (Figure 5b,d). Major SST increase occurs along the Eastern Beaufort Sea shelf (Figure 5f).
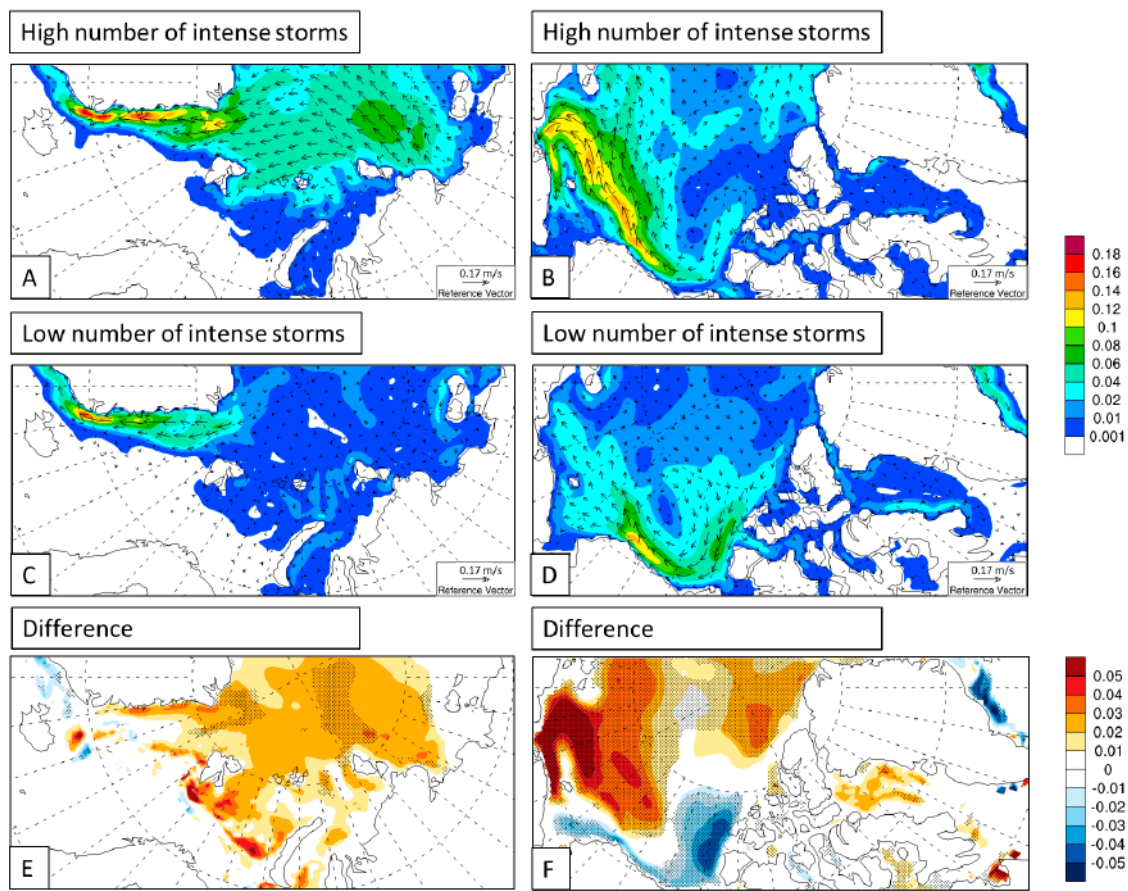
Figure 4. The composite analysis of sea level pressure (SLP; color shading) and near-surface wind (arrows) when the anomalously high count of the summer intense storms occurs over (**a**) the Atlantic Arctic Ocean; and (**b**) the Pacific Arctic Ocean, respectively, from 1948–2008. (**c**,**d**) are the same as (**a**,**b**) but for the anomalously low count of the summer intense storms. (**e**,**f**) show the differences between (**a**,**c**) and between (**b**,**d**), respectively. Units: hPa for SLP and m/s for wind. The differences at a confidence level of 95% are dotted.
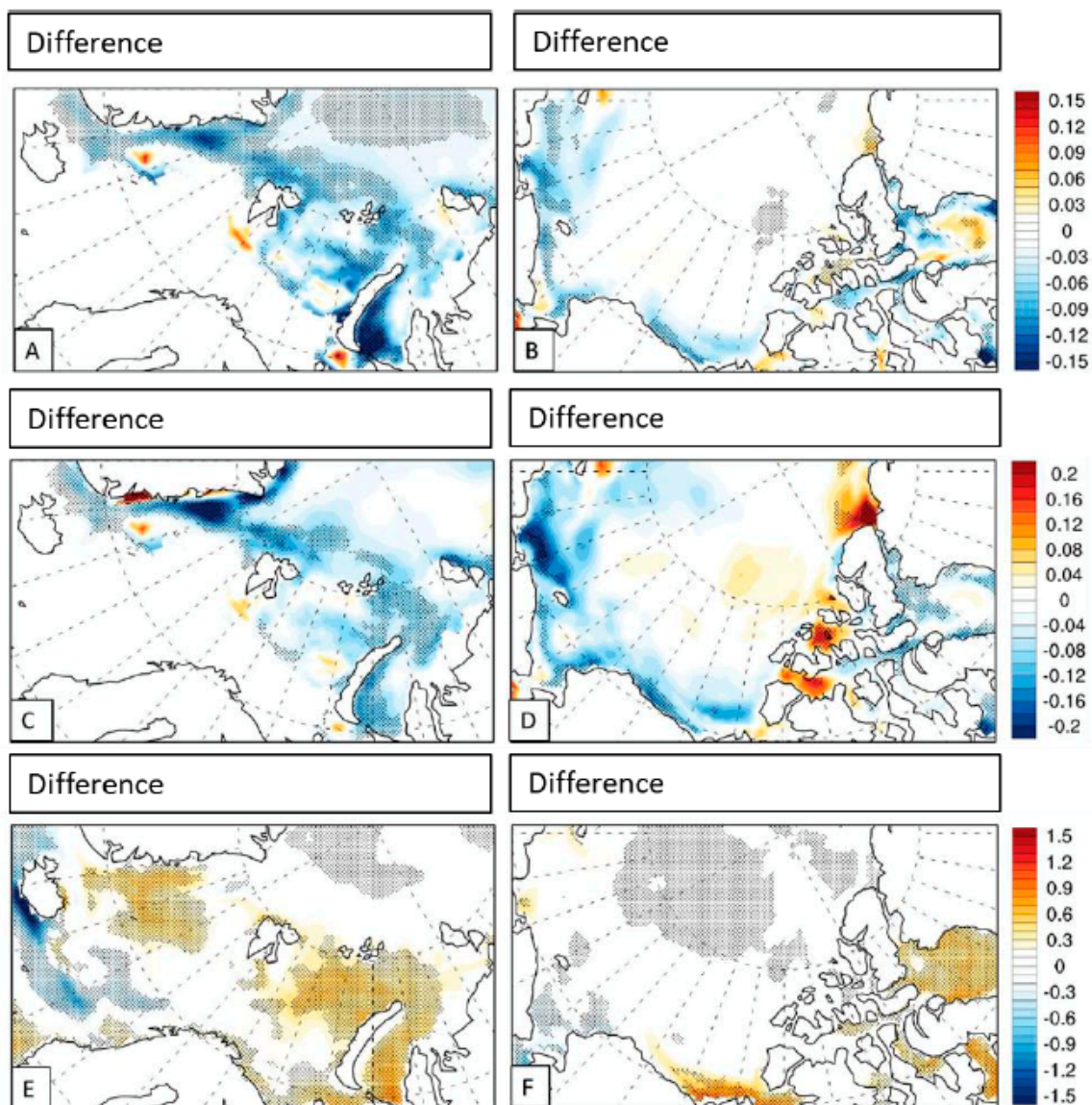
Figure 5. Differences of the composite analysis of sea-ice concentration (unit: %) between the anomalously high and low counts of the summer intense storms over (**a**) the Atlantic Arctic Ocean for the period of 1948–2008; and (**b**) the Pacific Arctic Ocean. (**c,d**) are the same as (a) and (b) but for sea ice thickness (unit: m). (**e,f**) are the same as (a) and (b) but for sea surface temperature (unit: °C). The values at a 95% confidence level are dotted.

To understand the changes in sea ice and SST identified above, we conducted the composite analysis for sea-ice motion and sea-ice energy budgets. Figure 6 shows the composite sea ice drift vectors and speed when the anomalously high and low intense storm count occurs, and their difference for the Atlantic and Pacific Arctic Ocean regions. In the Atlantic Arctic Ocean, there are obviously large sea-ice outflows from the Arctic Ocean, in particular from the Kara and Laptev Seas to the East Greenland Sea (Figure 6a), corresponding to the surface wind patterns associated with the high intense storm count as shown in Figure 4a. The comparable magnitude of the sea-ice velocity only occurs in the East Greenland Sea when there is a low number of the intense storms. The enhanced sea-ice export via Fram Strait associated with the more numerous intense storms dynamically contributes to the sea-ice loss in this area as shown in Figure 5a,c. On the other hand, the thinned ice would become vulnerable to wind forcing and further increase its velocity.
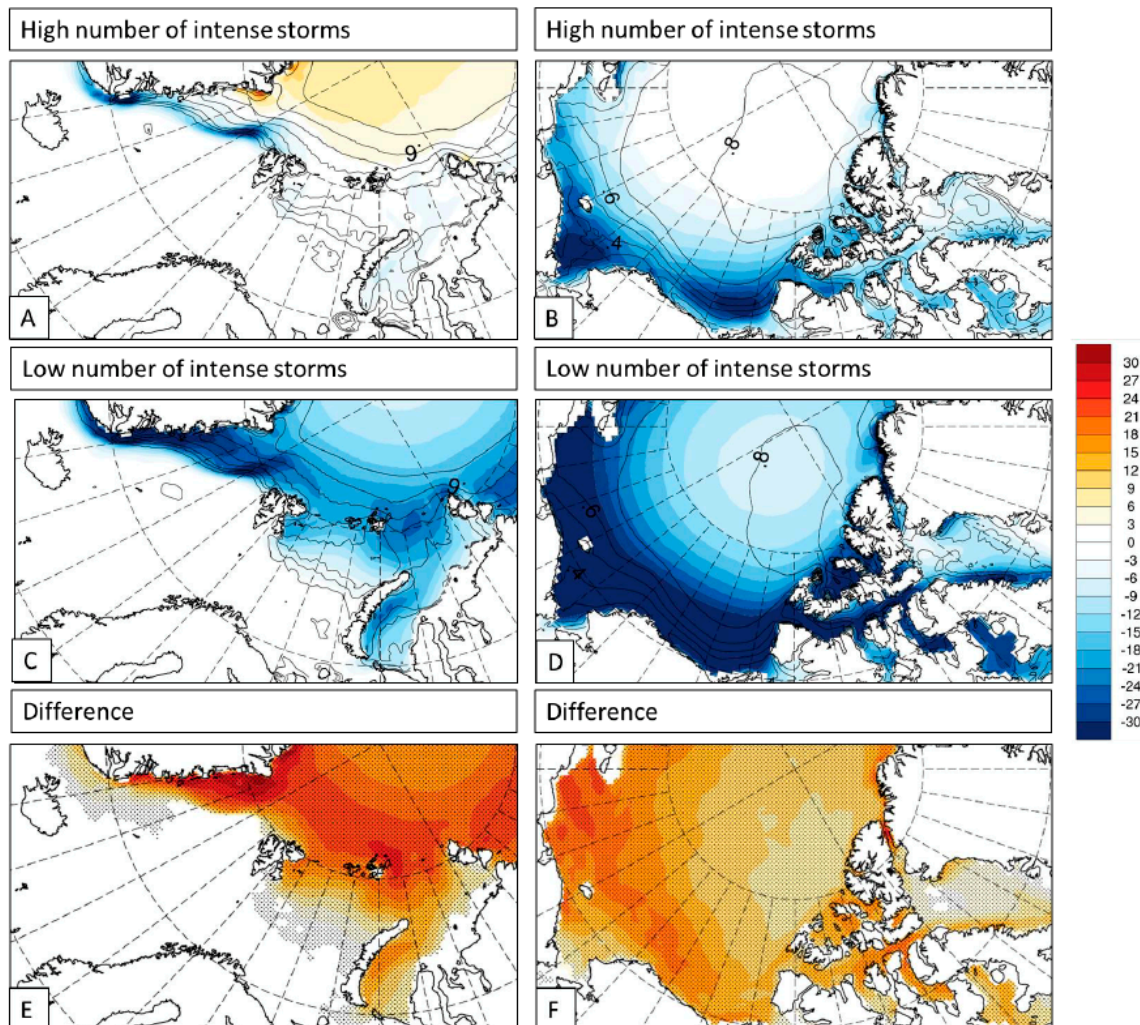
Figure 6. The same as Figure 4 but for sea ice drift (unit: (m/s)). The magnitude of sea ice drift speed is shaded in color. (**a**,**c**,**e**) show the composite analysis results in the Atlantic Arctic Ocean and (**b**,**d**,**f**) show those in the Pacific Arctic Ocean region specifically.

In the Pacific Arctic Ocean, when more numerous intense storms occur, a cyclonic sea-ice circulation appears in the Chukchi and East Siberian Seas, while the conventional Beaufort gyre shifts southeastward (Figure 6b). This is well consistent with the alteration of SLP and surface wind fields associated with the anomalously high number of intense storms as shown in Figure 4b. In the opposite case with the low number of intense storms, the Beaufort gyre expands to the north and northwest, forming an anticyclonic circulation in a large area of the Western Arctic. Compared to the latter, the former sea-ice circulation pattern reduces sea-ice transport from the thick ice area north of the Canadian Archipelago to the Beaufort–Chukchi Seas (Figure 6b), which contributes to the decrease in SIC and SIT in the latter areas (Figure 5b,d). However, there is an increase in sea-ice transport to the East Siberian Sea. The sea-ice circulation associated with the low number of intense storms (Figure 6d) obviously accounts for the SIT increase in the Canada Basin and the Canadian Archipelago (Figure 5d) due to the convergence effect of sea ice.

The composite analysis was continually extended to the net sea-ice heat fluxes, calculated as the difference between the net atmospheric surface heat fluxes and the oceanic heat flux of a model grid cell. The difference represents the net contribution from all radiative, sensible, and latent heat fluxes from the atmosphere and the turbulent heat flux from the ocean, indicating the total thermodynamic contribution to sea-ice changes (melt and growth). In this paper, we used the sign convention that negative (positive) net heat fluxes point downward (upward), which we can interpret as snow/ice melt (sea-ice growth).

When the high count of intense storms occurs over the Atlantic Arctic Ocean, a slightly negative value of the net sea-ice heat flux occurs in the Northern Barents Sea and the Kara Sea, and a large negative value appears along the sea-ice marginal zone in the East Greenland Sea (Figure 7a). There are

also small positive net sea-ice heat fluxes in the interior area of the study domain. This shows great difference from the case of the low count of intense storms, which exhibits an obviously larger negative value for the entire domain of the Atlantic Arctic Ocean (Figure 7c). The larger negative values, i.e., increased downward net sea-ice heat fluxes, indicate more sea-ice melt when less numerous intense storms occur. The same as these in the Atlantic Arctic Ocean, there are small (large) negative net sea-ice heat fluxes when more (less) numerous intense storms occur (Figure 7b,d). The decrease in the negative net sea-ice heat fluxes is further confirmed for both regions by the positive differences of the net sea-ice heat fluxes between the high and low counts of intense storms (Figure 7e,f).

Figure 7. The same as Figure 4, but for the net sea-ice heat fluxes (unit: W/m^2). Positive (negative) fluxes point upward (downward). (**a,c,e**) show the composite analysis results in the Atlantic Arctic Ocean and (**b,d,f**) show those in the Pacific Arctic Ocean region specifically.

According to the dynamic and thermodynamic analysis above, the large decrease in SIC and SIT in the Barents–Kara–Laptev Seas of the Atlantic Arctic and the Chukchi–Beaufort seas of the Pacific Arctic can obviously be attributed to the enhanced sea ice export from these areas, considering the decreased downward net sea ice heat flux and sea-ice melt, in the case of a high number of intense storms. However, the decreased SIC and SIT in the East Greenland Sea and the East Siberian Sea could not straightforwardly be explained because of the sea-ice import in these downstream areas of the changed sea ice transport and the decreased downward net heat fluxes and sea-ice melt. The decrease in SIC and SIT in these areas may be ascribed to prior conditions before intense storms occur, which the composite analysis here may not be able to reveal. For example, these areas are under influences of

storm tracks, and many storms travel through these areas before they reach the criterion of intense storms used for the composite analysis. This transient effect needs to be examined to understand storm impacts on sea ice during their different development phases and would be a follow-up study.

The dynamic and thermodynamic analysis results here augment existing case studies or statistical analysis about sea-ice changes associated with storms [24,51]. Nevertheless, we have only analyzed overall changes in dynamics and thermodynamics here. Better understanding of storm impacts on underlying sea ice and ocean as well as associated interactions between them need further detailed energy budget analyses, in particular associated with finer scale processes. For example, reduced downward shortwave radiation due to increased cloudiness and increased upward turbulent fluxes due to break-up of temperature inversions and destabilization of the boundary layer may contribute to the decreased downward net sea-ice surface heat fluxes (including radiative fluxes and turbulent fluxes) and reduced sea-ice melt rates when numerous intense storms occur, as shown in Figure 7. Storm-induced cloudiness seasonally changes partitioning of downward shortwave and longwave radiation fluxes, altering surface energy budgets. Intense storm may also break up pack ice and subsequently increase open water to enhance air–sea heat exchange and albedo feedback, which may further influence sea-ice energy budgets and sea-ice melt and growth.

4. Summary and Discussions

Intense and long-lasting storms have more frequently occurred over the Arctic Ocean, which have obviously caused or contributed to the occurrence of extreme events, including record lows of sea-ice extents in summer and record highs of warm temperature in winters [24–28]. To understand intense and long-lasting storms and identify sources of their predictability, detailed observational and modeling studies have revealed that these Arctic storms have demonstrated unique dynamic and thermodynamic structures and driving mechanisms [19,20,22,23], different from their midlatitude counterpart [52].

Although the recently occurring intense storms show tight linkage with the record lows of summer sea ice extent, it remains unclear how all intense storms have integratively contributed to the observed long-term changes in sea ice and what physical processes are behind these contributions. We therefore analyzed ensemble hindcast simulations by the coupled Arctic regional model HIRHAM–NAOSIM, which allows atmosphere–sea ice–ocean interactions so that feedback processes are involved in the temporal co-development of storms, sea ice, and ocean. The 61-year-long model analysis focused on the summer ice-melting period from 1 July to 15 September.

The results indicate that the model realistically simulated the regional characteristics of climatological storm activity, characterized by the storm count and intensity. The simulated storm count captures the variability derived from the NCEP–NCAR reanalysis, though the simulated one is higher than that in the reanalysis, which could be attributed to the higher resolution of the model that may better represent smaller and shallower cyclones. Comparison across different subregions indicates that the Central Arctic generally has a higher storm count but weaker storm intensity. However, there are less numerous storms but with stronger intensity over the surrounding shelf seas. This would be due to larger baroclinicity in the shelf seas, resulting from the thermal contrast between open water and sea ice or between the partially sea-ice covered seas and adjacent landmass.

Generally, more numerous intense storms and the largest sea-ice changes occur in the North Atlantic and North Pacific Arctic Ocean. Thus, the analysis about impacts of storms on sea ice focused on these two subregions. A composite analysis indicates a larger decrease in sea-ice concentration and thickness in the Barents and Kara Seas and the Chukchi and East Siberian Seas, respectively, when more numerous intense storms occur over the North Atlantic and North Pacific Arctic Ocean. To understand the underlying physical processes behind these sea-ice changes, we further conducted the composite analysis on sea-ice motions and net sea-ice heat budgets. The results exhibit an increased sea-ice transport from the Barents–Kara–Laptev Seas towards the East Greenland Sea under influence of numerous intense Atlantic Arctic storms, resulting in a decrease of sea ice in the former areas.

The weakened sea-ice transport from the thick ice area north of the Canadian Archipelago led to a decrease of sea ice in the Chukchi–East-Siberian Seas under influence of numerous intense Pacific Arctic storms.

Our study stresses the importance of the changed sea-ice dynamics driven by surface winds associated with intense storms especially for the Barents–Kara–Laptev Seas and the Chukchi–Beaufort Seas, which is consistent with previous studies about impacts of large scale atmospheric circulation [1,53]. The composite analysis of the net sea-ice heat budget shows that substantially decreased downward fluxes in the case of high intense storm count occurs, compared with that of low intense storm count, in both the North Atlantic and North Pacific Arctic Oceans. This is interpreted by two storm-driven mechanisms, the increased cloudiness and subsequently reduced downward shortwave radiation (or reduced net downward radiation due to seasonally-dependent partitioning between shortwave and longwave radiation by cloudiness) and the destabilization of the boundary layer and subsequently increased upward turbulent fluxes. A detailed, quantitative analysis of all these processes is beyond the scope of this paper. In addition, our study here was based on a period from 1948–2008. Since 2008, Arctic sea ice has experienced a drastic loss. Thermodynamics and dynamics associated with storm impact on sea ice during these most recent years have not been well investigated. All of these will be a follow-up research with new model simulations and new observational datasets.

The consequence of our composite results is, on the one hand, that the reduced sea-ice cover in the specified regions by intense storms is mainly dynamically driven, which leads to ice transport/export into other regions. On the other hand, the reduced sea-ice cover can have an important feedback to intense storm development. To distinguish if numerous intense storms are the cause or effect of sea-ice reduction cannot be discussed with the applied composite approach. This complex interaction between storms and sea ice, which involve many competing and time-lagged processes, needs definitively further investigations. Importantly, a recent study found both negative (more cyclones ~ smaller ice extent) and positive (more cyclones ~ larger ice extent) correlation between summer (May–September) cyclone characteristics and September sea-ice extent [54]. They showed that the results depend on the considered summer month and period, data set, and model set up (resolution, atmosphere-alone or coupled). New observations, such as those from the year-round Multidisciplinary drifting Observatory for the Study of Arctic Climate (MOSAiC) and more comprehensive and higher-resolution model simulations will provide more detailed process understanding of this in the future.

Author Contributions: X.Z. conceived the research and advised the student A.S.; X.Z. and A.R. organized the collaborative research; A.R., W.D., and K.D. designed and conducted the model simulations; A.S. did statistical computation of the model data analysis, plotted figures, and wrote initial draft; X.Z., A.R., W.D., and K.D. re-analyzed the data and substantially revised/rewrote the paper.

Conflicts of Interest: The authors declare no conflict of interest.

References

1. Zhang, X.; Sorteberg, A.; Zhang, J.; Gerdes, R.; Comiso, J.C. Recent radical shifts in atmospheric circulations and rapid changes in Arctic climate system. *Geophys. Res. Lett.* **2008**, *35*, L22701. [CrossRef]
2. Huang, J.; Zhang, X.; Zhang, Q.; Lin, Y.; Hao, M.; Luo, Y.; Zhao, Z.; Yao, Y.; Chen, X.; Wang, L.; et al. Recently amplified arctic warming has contributed to a continual global warming trend. *Nat. Clim. Chang.* **2017**, *7*, 875–880. [CrossRef]

3. Comiso, J.C.; Parkinson, C.L.; Gersten, R.; Stock, L. Accelerated decline in the Arctic sea ice cover. *Geophys. Res. Lett.* **2008**, *35*, L01703. [CrossRef]

4. Kwok, R.; Rothrock, D.A. Decline in Arctic sea ice thickness from submarine and ICESat records: 1958–2008. *Geophys. Res. Lett.* **2009**, *36*, L15501. [CrossRef]

5. Sato, K.; Inoue, J.; Watanabe, M. Influence of the Gulf Stream on the Barents Sea ice retreat and Eurasian coldness during early winter. *Environ. Res. Lett.* **2014**, *9*, 084009. [CrossRef]

6. Stroeve, J.C.; Serreze, M.C.; Holland, M.M.; Kay, J.E.; Maslanik, J.; Barrett, A.P. The Arctics rapidly shrinking sea ice cover: A research synthesis. *Clim. Chang.* **2011**, *110*, 1005–1027. [CrossRef]

7. Thompson, D.W.J.; Wallace, J.M. The Arctic Oscillation signature in the wintertime geopotential height and temperature fields. *Geophys. Res. Lett.* **1998**, *25*, 1297–1300. [CrossRef]

8. Zhang, X.; Walsh, J.E.; Zhang, J.; Bhatt, U.S.; Ikeda, M. Climatology and interannual variability of Arctic cyclone activity, 1948–2002. *J. Clim.* **2004**, *17*, 2300–2317. [CrossRef]

9. Sepp, M.; Jaagus, J. Changes in the activity and tracks of Arctic cyclones. *Clim. Chang.* **2011**, *105*, 577–595. [CrossRef]

10. Inoue, J.; Hori, M.E. Arctic cyclogenesis at the marginal ice zone: A contributory mechanism for the temperature amplification? *Geophys. Res. Lett.* **2011**, *38*, L12502. [CrossRef]

11. Inoue, J.; Hori, M.E.; Takaya, K. The role of Barents Sea ice in the wintertime cyclone track and emergence of a warm-Arctic cold-Siberian anomaly. *J. Clim.* **2012**, *25*, 2561–2568. [CrossRef]

12. Basu, S.; Zhang, X.; Wang, Z. Eurasian winter storm activity at the end of the century: A CMIP5 multi-model ensemble projection. *Earths Future* **2018**, *6*, 61–70. [CrossRef]

13. Day, J.J.; Holland, M.; Hodges, K.I. Seasonal differences in the response of Arctic cyclones to climate change in CESM1. *Clim. Dyn.* **2018**, *50*, 3885–3903. [CrossRef]

14. Rigor, I.G.; Wallace, J.M.; Colony, R.L. Response of Sea Ice to the Arctic Oscillation. *J. Clim.* **2002**, *15*, 2648–2663. [CrossRef]

15. Zhang, X.; Ikeda, M.; Walsh, J.E. Arctic sea ice and freshwater changes driven by the atmospheric leading mode in a coupled sea ice-ocean model. *J. Clim.* **2003**, *16*, 2159–2177. [CrossRef]

16. Simmonds, I.; Burke, C.; Keay, K. Arctic climate change as manifest in cyclone behavior. *J. Clim.* **2008**, *21*, 5777–5796. [CrossRef]

17. Kriegsmann, A.; Brümmer, B. Cyclone impact on sea ice in the central Arctic Ocean: A statistical study. *Cryosphere* **2014**, *8*, 303–317. [CrossRef]

18. Boisvert, L.N.; Petty, A.A.; Stroeve, J.C. The impact of the extreme winter 2015/16 Arctic cyclone on the Barents-Kara seas. *Mon. Weather Rev.* **2016**, *144*, 4279–4287. [CrossRef]

19. Tanaka, H.L.; Yamagami, A.; Takahashi, S. The structure and behavior of the arctic cyclone in summer analyzed by the JRA-25/JCDAS data. *Polar Sci.* **2012**, *6*, 44–69. [CrossRef]

20. Aizawa, T.; Tanaka, H.L. Axisymmetric structure of the long lasting summer Arctic cyclones. *Polar Sci.* **2016**, *10*, 192–198. [CrossRef]

21. Rinke, A.; Maturilli, M.; Graham, R.M.; Matthes, H.; Handorf, D.; Cohen, L.; Hudson, S.R.; Moore, J.C. Extreme cyclone events in the Arctic: Wintertime variability and trends. *Environ. Res. Lett.* **2017**, *12*, 094006. [CrossRef]

22. Tao, W.; Zhang, J.; Zhang, X. The role of stratosphere vortex downward intrusion in a long-lasting late-summer Arctic storm. *Q. J. R. Meteorol. Soc.* **2017**, *143*, 1953–1966. [CrossRef]

23. Tao, W.; Zhang, J.; Zhang, X. Driving roles of tropospheric and stratospheric thermal anomalies in the intensification and persistence of 2012 Arctic superstorm. *Geophys. Res. Lett.* **2017**, *44*, 10017–10025. [CrossRef]

24. Simmonds, I.; Rudeva, I. The great Arctic cyclone of August 2012. *Geophys. Res. Lett.* **2012**, *39*, L23709. [CrossRef]

25. Zhang, J.; Lindsay, R.; Schweiger, A.; Steele, M. The impact of an intense summer cyclone on 2012 Arctic sea ice retreat. *Geophys. Res. Lett.* **2013**, *40*, 720–726. [CrossRef]

26. Moore, G.W.K. The December 2015 North Pole warming event and the increasing occurrence of such events. *Sci. Rep.* **2016**, *6*, 39084. [CrossRef]

27. Graham, R.M.; Cohen, L.; Petty, A.A.; Boisvert, L.N.; Rinke, A.; Hudson, S.R.; Nicolaus, M.; Granskog, M.A. Increasing frequency and duration of Arctic winter warming events. *Geophys. Res. Lett.* **2017**, *44*, 6974–6983. [CrossRef]

28. Kim, B.-K.; Hong, J.-Y.; Jun, S.-Y.; Zhang, X.; Kwon, H.; Kim, S.-J.; Kim, J.-H.; Kim, S.-W.; Kim, H.-K. Major cause of unprecedented Arctic warming in January 2016: Critical role of an Atlantic windstorm. *Sci. Rep.* **2017**, *7*, 40051. [CrossRef]

29. Zhang, X.; He, J.; Zhang, J.; Polyakov, I.; Gerdes, R.; Inoue, J.; Wu, P. Enhanced poleward moisture transport and amplified northern high-latitude wetting trend. *Nat. Clim. Chang.* **2013**, *3*, 47–51. [CrossRef]

30. Vihma, T. Effects of Arctic sea ice decline on weather and climate: A review. *Surv. Geophys.* **2014**, *35*, 1175–1214. [CrossRef]

31. Brümmer, B.; Múller, G.; Hoeber, H. A Fram Strait cyclone: Properties and impact on ice drift as measured by aircraft and buoys. *J. Geophys. Res.* **2003**, *108*. [CrossRef]

32. Asplin, M.G.; Galley, R.; Barber, D.G.; Prinsenberg, S. Fracture of summer perennial sea ice by ocean swell as a result of Arctic storms. *J. Geophys. Res.* **2012**, *117*, C06025. [CrossRef]

33. Wei, J.; Zhang, X.; Wang, Z. Impacts of extratropical storm tracks on Arctic sea ice export through Fram Strait. *Clim. Dyn.* **2019**, *52*, 2235–2246. [CrossRef]

34. Serreze, M.C.; Barrett, A.P. The summer cyclone maximum over the central Arctic Ocean. *J. Clim.* **2008**, *21*, 1048–1065. [CrossRef]

35. Dorn, W.; Dethloff, K.; Rinke, A. Improved simulation feedbacks between atmosphere and sea ice cover over the Arctic Ocean in a coupled regional climate model. *Ocean Model.* **2009**, *29*, 103–114. [CrossRef]

36. Kalnay, E.; Kanamitsu, M.; Kistler, R.; Collins, W.; Deaven, D.; Gandin, L.; Iredell, M.; Saha, S.; White, G.; Woollen, J.; et al. The NCEP/NCAR 40-year reanalysis project. *Bull. Am. Meteorol. Soc.* **1996**, *77*, 437–471. [CrossRef]

37. Dorn, W.; Dethloff, K.; Rinke, A. Limitations of a coupled regional climate model in the reproduction of the observed Arctic sea ice retreat. *Cryosphere* **2012**, *6*, 985–998. [CrossRef]

38. Rinke, A.; Dethloff, K.; Dorn, W.; Handorf, D.; Moore, J.C. Simulated Arctic atmospheric feedbacks associated with late summer sea ice anomalies. *J. Geophys. Res. Atmos.* **2013**, *118*. [CrossRef]

39. Jaiser, R.; Dethloff, K.; Handorf, D.; Rinke, A.; Cohen, J. Impact of sea ice cover changes on the Northern Hemisphere atmospheric winter circulation. *Tellus* **2012**, *64*, 11595. [CrossRef]

40. Zhang, X.; Lu, C.; Guan, Z. Weakened cyclones, intensified anticyclones, and the recent extreme cold winter weather events in Eurasia. *Environ. Res. Lett.* **2012**, *7*, 044044. [CrossRef]

41. Akperov, M.G.; Mokhov, I.I.; Rinke, A.; Dethloff, K.; Matthes, H. Cyclones and their possible changes in the Arctic by the end of the 21st century from regional climate model simulations. *Theor. Meteorol. Clim.* **2015**, *122*, 85–96. [CrossRef]

42. Tilinina, N.; Gulev, S.K.; Bromwich, D.H. New view of Arctic cyclone activity from the Arctic system reanalysis. *Geophys. Res. Lett.* **2014**, *41*, 1766–1772. [CrossRef]

43. Akperov, M.; Rinke, A.; Mokhov, I.I.; Matthes, H.; Semenov, V.A.; Adakudlu, M.; Cassano, J.; Christensen, J.H.; Dembitskaya, M.A.; Dethloff, K.; et al. Cyclone activity in the Arctic from an ensemble of regional climate models (Arctic CORDEX). *J. Geophys. Res. Atmos.* **2018**, *123*, 2537–2554. [CrossRef]

44. Bromwich, D.H.; Hines, K.M.; Bai, L.-S. Development and testing of Polar WRF: 2. Arctic Ocean. *J. Geophys. Res.* **2009**, *114*, D08122. [CrossRef]

45. Bromwich, D.H.; Wilson, A.B.; Bai, L.-S.; Liu, Z.; Barlage, M.; Shih, C.-F.; Maldonado, S.; Hines, K.M.; Wang, S.H.; Woollen, J.; et al. The Arctic system reanalysis version 2. *Bull. Am. Meteorol. Soc.* **2017**, *99*, 805–828. [CrossRef]

46. Zahn, M.; Akperov, M.; Rinke, A.; Feser, F.; Mokhov, I.I. Trends of cyclone characteristics in the Arctic and their patterns from different reanalysis data. *J. Geophys. Res. Atmos.* **2018**, *123*, 2737–2751. [CrossRef]

47. Vinje, T. Fram Strait ice fluxes and atmospheric circulation 1950–2000. *J. Clim.* **2001**, *14*, 3508–3517. [CrossRef]

48. Overland, J.E. Meteorology of the Beaufort Sea. *J. Geophys. Res.* **2009**, *114*, C00A07. [CrossRef]

49. Serreze, M.C.; Barrett, A.P. Characteristics of the Beaufort Sea high. *J. Clim.* **2011**, *24*, 159–182. [CrossRef]

50. Wu, Q.; Zhang, J.; Zhang, X.; Tao, W. Interannual variability and long-term changes of atmospheric circulation over the Chukchi and Beaufort seas. *J. Clim.* **2014**, *27*, 4871–4889. [CrossRef]

51. Parkinson, C.L.; Comiso, J.C. On the 2012 record low Arctic sea ice cover: Combined impact of preconditioning and an August storm. *Geophys. Res. Lett.* **2012**, *40*, 1356–1361. [CrossRef]

52. Bluestein, H.B. *Synoptic-Dynamic Meteorology in Midlatitudes, Observations and Theory of Weather Systems*; Oxford University Press: Oxford, UK, 1993; Volume 2, 594p.

53. Ogi, M.; Yamazaki, K.; Wallace, J.M. Influence of winter and summer surface wind anomalies on summer Arctic sea ice extent. *Geophys. Res. Lett.* **2010**, *37*, L07701. [CrossRef]

54. Rae, J.G.L.; Todd, A.D.; Blockley, E.W.; Ridley, J.K. How much should we believe correlations between Arctic cyclones and sea ice extent? *Cryosphere* **2017**, *11*, 3023–3034. [CrossRef]